JOURNAL OF CATALYSIS 18, 57–69 (1970)

Chemisorption Rates by Chromatography—Hydrogen on Cobalt

J. C. ADRIAN AND J. M. SMITH

University of California, Davis, California 95616

Received October 2, 1969

Chemisorption rates for hydrogen on a cobalt/kieselguhr catalyst were measured by a chromatographic technique. Using deuterium as a tracer with continuous flow of hydrogen ensured that the rates corresponded to constant surface coverage. Data were obtained at atmospheric pressure over the range −34 to 23.5°C. The method could not be applied at high temperatures because of nonequilibrium behavior, possibly due to tightly bound hydrogen which was not desorbable at low temperature.

The equilibrium adsorption from −34 to 23.5°C was 4–5 times less than that for a similar nickel/kieselguhr catalyst. The rates of adsorption of hydrogen on nickel and cobalt were about equal at the lower temperature level but that for cobalt was an order of magnitude less at 23.5°C. The corresponding activation energies were 5.2 kcal/g mole (cobalt) and 13.8 (nickel). These differences were much greater than expected from the difference in surface area for the two catalysts.

Based upon the theory of Kubin (*3*) for the transient behavior of a packed column of adsorbent particles, a method (*8*) has been developed for evaluating rate and equilibrium parameters in the column from chromatographic curves. The critical point in the method is that all the mass transport processes, including the adsorption rate at the adsorption site, must be linear. Chemisorption rates normally do not satisfy this requirement over a significant concentration range. By using an isotope technique, Padberg and Smith (*7*) have shown that pseudolinearity can be achieved, and they evaluated chemisorption rates for hydrogen on a nickel catalyst by the chromatographic method. Cobalt also readily adsorbs hydrogen by a dissociative mechanism and supported cobalt is a common hydrogenation catalyst. As a step in building up knowledge about chemisorption, rates are reported here for a commercial cobalt–on–kieselguhr catalyst. Rates were evaluated from −34 to 23.5°C at atmospheric pressure by analysis of the chromatographic peaks observed when a pulse of deuterium is introduced into the column of catalyst particles.

The method is based upon operating at a constant, high, surface coverage of hydrogen on the catalyst. This is obtained by continuous flow of hydrogen through the column, so that all the sites available at the column temperature are occupied. If a pulse of deuterium is then introduced, it will be chemisorbed in proportion to its fraction in the gas stream. The deuterium is thus retained for a period, and its retention time is a measure of the equilibrium distribution between the gas phase and the cobalt surface. Since the chemisorption is dissociative, the adsorption–desorption process will establish equilibrium between H_2, D_2, and HD in the gas phase by the rapid exchange reaction, $H_2 + D_2 = 2HD$ (*4*, *5*).

The dispersion of the deuterium peak as it travels through the column is determined by the rate of chemisorption and rates of the other transport processes. Ozaki *et al.* (*4*, *5*), and Padberg and Smith (*7*) have shown that the equilibrium adsorption of

hydrogen and deuterium on nickel catalysts are essentially the same. If the isotope effect on the rates is also negligible, the dispersion data will give the chemisorption rates of hydrogen.

Since the total pressure is constant and the overall hydrogen plus deuterium system is at equilibrium at all times, the total rates of adsorption and desorption are equal. That is, the process is carried out at a single point on the nonlinear isotherm. The situation is depicted in Fig. 1 where isotherms are shown schematically for three temperatures. At T_1 the entire column will be at point A_1 corresponding to a saturated condition at nearly complete coverage in the flat portion of the isotherm. Therefore, the net rate of adsorption of deuterium can be represented by the *linear* equation

$$\frac{dn_a}{dt} = r_a - r_d = k_a C - \frac{k_a}{K_a} n_a. \qquad (1)$$

Here K_a is not the true adsorption equilibrium constant determined from a linear isotherm, but rather a pseudo-equilibrium constant defined as the ratio of n_a to C at point A_1. In order to eliminate the uncertainty of whether the deuterium in the gas is present as HD or D_2, the deuterium concentration in Eq. (1) is defined as

$$C = \tfrac{1}{2}C_{HD} + C_{D_2}. \qquad (2)$$

Method of Analysis

Kubin (*3*) was able to relate the transform of the differential equations describing the mass transport of tracer (deuterium in our case) in the column of particles to the moments of the chromatographic peak at the exit. The equations take into account axial dispersion in the gas phase in the column (E_A), transfer of tracer from gas phase to outer surface of a particle (k_f), intraparticle diffusivity (D_i), and adsorption at an interior site on the catalyst surface (k_a). The terms in parentheses represent the corresponding rate parameters. The differential equations, and boundary and initial conditions, are given elsewhere (*6*). The major assumptions are no radial gradients in the column, square pulse input, and spherical particles of constant radius R. The final equations relating the moments of the column to the rate parameters are as follows:

$$(\mu'_1)_{Col} = \frac{z}{v}(1 + \delta_0) + \frac{1}{2}t_0. \qquad (3)$$

$$(\mu_2)_{Col} = \frac{2z}{v}\left[\delta_1 + \frac{E_A}{\alpha}(1 + \delta_0)^2\left(\frac{1}{v}\right)^2\right] + \frac{1}{12}t_0^2, \qquad (4)$$

where

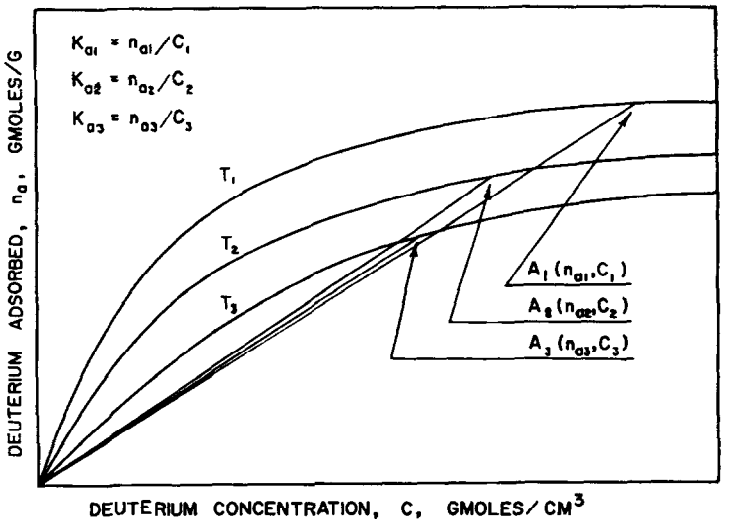

FIG. 1. Schematic adsorption isotherms.

$$\delta_0 = \frac{1-\alpha}{\alpha}\beta\left(1+\frac{\rho_p}{\beta}K_a\right), \tag{5}$$

$$\delta_0 = \frac{1-\alpha}{\alpha}\beta\left[\frac{\rho_p}{\beta}\frac{K_a^2}{k_a}+\frac{R^2\beta}{15}\left(1+\frac{\rho_p}{\beta}K_a\right)^2\left(\frac{1}{D_i}+\frac{5}{k_fR}\right)\right]. \tag{6}$$

The first absolute moment μ'_1 can be obtained from the measured chromatographic peak $C(z, t)$ by the expression

$$\mu'_1 = \frac{\int_0^\infty t\,C(z,t)\,dt}{\int_0^\infty C(z,t)\,dt} \tag{7}$$

Similarly, the second, central moment is given by

$$\mu_2 = \frac{\int_0^\infty (t-\mu'_1)^2\,C(z,t)\,dt}{\int_0^\infty C(z,t)\,dt}. \tag{8}$$

In brief, the method of analysis involves using values of μ'_1 and μ_2, obtained from the measured chromatographs, in Eqs. (3)–(6) to determine the rate parameters. In our case the rate constant for chemisorption k_a is the major objective.

Experimental Methods

Pulses of deuterium were introduced into the steady stream of hydrogen flowing through the column and chromatographic curves measured for three average particle sizes ($R = 0.229$, 0.185, and 0.105 mm). Runs were made at several interparticle gas velocities in the range 2–22 cm/sec (at column temperature and 1 atm). The temperature range for which rates of chemisorption were calculated was 23.5 to −34°C. This range was chosen on the basis of results from preliminary measurements, as described later.

The apparatus (Fig. 2) was a conventional chromatograph (with thermal conductivity detector) modified so that the adsorption column contained the cobalt catalyst. Pulse volumes of 1.0 cm³ were introduced through a 7-port gas sampling device. Deviations from a square-wave input pulse and dispersion between column and detector were measured and found to be negligible. The column was connected to the sample valve and the detector by a total length of 40 cm of ⅛-in. nominal i.d. copper tubing. The columns themselves were nominal ¼-in. copper tubing, with dimensions as given in Table 2.

To correct for deviations from a square-wave injection and retention of the pulse between sample injection and column entrance and column exit and detector, retention times were determined for pulses of helium (nonadsorbable) introduced into the hydrogen stream.

Residual traces of oxygen were removed from the prepurified hydrogen (Matheson Co., stated purity 99.95%) by an Englehard Deoxo unit (Fig. 2). The helium used (General Dynamics Co., stated purity 99.99%) was also passed through the Deoxo unit during the reduction of the catalyst particles. The technical grade deuterium (Matheson Co., purity 98%) was used without further treatment.

Catalyst Particles

The particles were Girdler Corporation, hydrogenation Catalyst (G-61) consisting of 60 wt % cobalt (in oxidized form) on kieselguhr. The particles were prepared by crushing and sieving ⅜ × ¼-in. tablets. The catalyst was reduced in place by a two-step process: (i) a slow flow (10 cm³/min) of helium was passed through the column, held at 460°C, for 2 hr; (ii), then the helium flow was gradually replaced with a hydrogen flow of 30 cm³/min, and the column was held at 415°C for 15 hr. Before and between experiments, a continuous stream of hydrogen was passed through the column. Preliminary experiments showed that the final results were sensitive to variations in the reduction procedure.

The properties of the catalyst particles are given in Table 1. The particle density, ρ_p, and porosity due to pores of radii greater than 175 Å were determined in an Aminco mercury porosimeter. The pressure limitation of the instrument prevented filling pores smaller than $a = 175$ Å with mercury. The pore-volume distribution for $a > 175$ Å was also established from the porosimeter

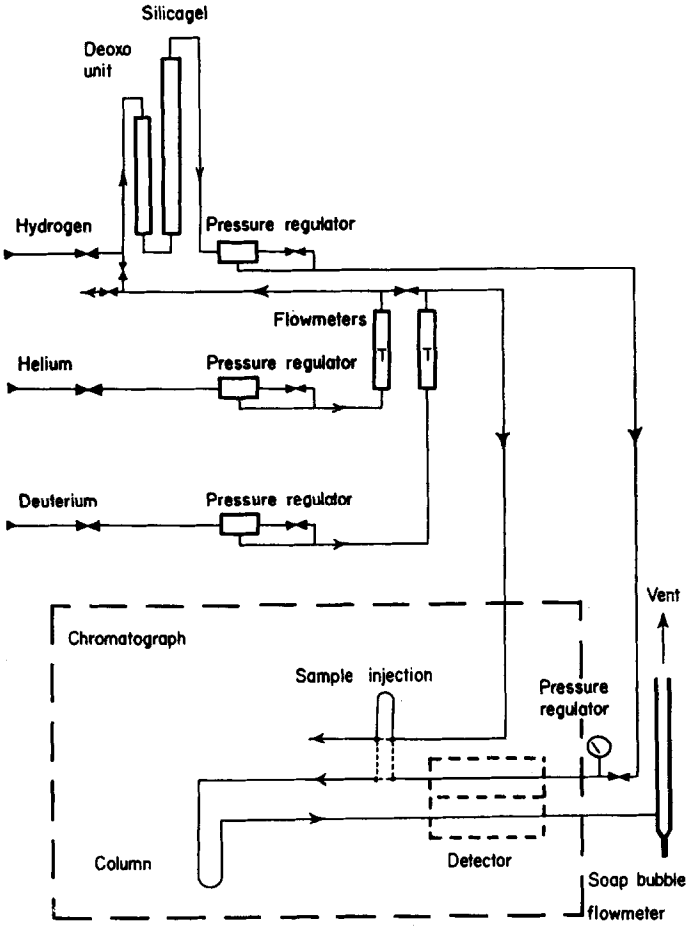

FIG. 2. Flow diagram of the apparatus.

data. The most probable radius of the macropores was greater than 175 Å. It was found to be 200 Å by identifying the inflection point of the penetration versus pore radius curve. However, the minimum in the pore-size distribution curve was at a radius less than 175 Å. It was estimated to be about 60 Å. If this latter radius is taken as the division between macro- and micropores, the macropore porosity is 0.39.

The true solid density was measured in a Beckman pycnometer using helium. From the particle and true densities the total particle porosity ($\beta = 0.64$) was established. Then the porosity of the micropore region was obtained by difference. The particle density obtained from the porosimeter (by mercury displacement at atmospheric pressure) was checked by using the pycnometer with a sample whose pores were filled with water. This latter method gave $\rho_p = 1.77$ g/cm^3, versus 1.74 by the porosimeter method.

The total surface area was determined by the dynamic method (with a Perkin-Elmer Sorptometer), using nitrogen adsorption at liquid nitrogen temperature. Since this area is almost exclusively in the micropores, the average micropore radius was calculated using the micropore porosity (or pore volume, V_i) and the equation $\bar{a}_i = 2V_i/S_g$.

Columns Used

The characteristics of the columns of particles is given in Table 2. The lengths were chosen so as to cover the velocity range 2–22 cm/sec with a pressure drop of 10–30

TABLE 1
PROPERTIES OF CATALYST PARTICLES

	Reduced	Unreduced
Cobalt content (wt %)	74.	60.
Particle density (g/cm³)	1.74	2.04
True solid density (g/cm³)	4.79	5.88
Porosity of pores for $a > 175$ Å	0.26	0.21
Porosity of macropores ($a > 60$ Å)	0.39	
Total porosity of particles	0.64	
Porosity of micropores ($a < 60$ Å)	0.25	
Most probable radius of macropores $\bar{a}_a$ (Å)	200.	
Av radius of micropores $\bar{a}_i$ (Å)	37.	
Surface area (m²/g)	77.	

in. of water. For the largest particles (Col I) three individually reduced batches were used to evaluate the reproducibility of the moments. The interparticle porosity α is a somewhat sensitive parameter in Eqs. (5) and (6) and should be measured as accurately as possible. The values given in Table 2 were determined from the particle density, mass of catalyst in the column, and the column volume. The latter was estimated from the diameter and packed length.

Typical Chromatographs

Figure 3 illustrates the type of chromatographic peaks obtained for three temperatures. The curves are for approximately the same velocity and also include helium peaks to show the retention time and extent of dispersion for a nonadsorbable gas. The difference in dispersion between helium and deuterium peaks is more pronounced than indicated because the two peaks were measured at different recorder attenuations. The deuterium peaks have retention time only slightly affected by temperature. Since the retention is a measure of the equilibrium absorption, this result is in agreement with the concepts shown in Fig. 1; that is, the pseudoequilibrium constant does not change much with temperature. However, there is a distinct increase in breadth of the curves as the temperature decreases. Since the mass transport parameters (E_A, k_f, and D_i) are not particularly sensitive to temperature, it is anticipated that this increase in dispersion is indeed due to the decrease in rate of chemisorption. Such broadening or tailing also could be caused by nonlinearity in the system. A test for this is to see if the moments of the chromatographic curves change with sample size. Padberg and Smith (7) did this with a nickel catalyst and found a negligible

TABLE 2
COLUMN CHARACTERISTICS AND OPERATING CONDITIONS

	Col I			Col II	Col III
	Batch 1	Batch 2	Batch 3		
Range of sieve openings (mm)	0.495–0.701	0.495–0.701	0.495–0.701	0.246–0.495	0.175–0.246
Av particle radius, R (mm)	0.299	0.299	0.299	0.185	0.105
Mass of catalyst reduced (g)	8.56	8.23	8.24	5.15	3.43
Col i.d. (cm)	0.481	0.481	0.481	0.481	0.481
Col length[a] (cm)	40.	40.	40.	30.	20.
Interparticle porosity α	0.42	0.45	0.45	0.46	0.46
Temp range (°C)	200–300	0–75	200, −34 to 23.5	−34 to 23.5	−34 to 23.5

[a] Length packed with particles.

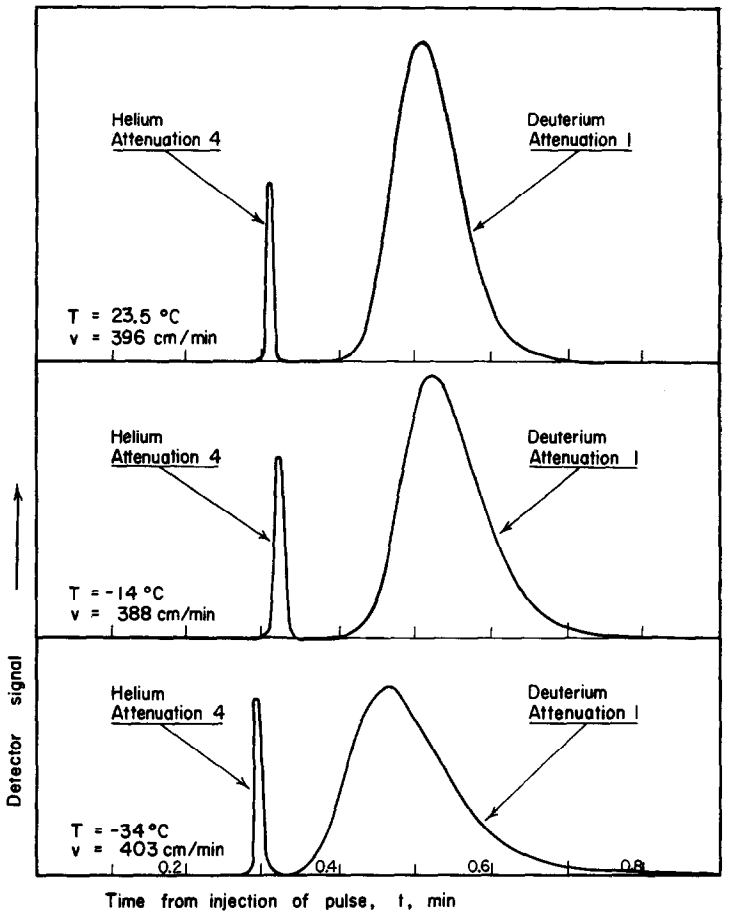

FIG. 3. Typical chromatographs (Col III, R = 0.105 mm).

change. It will be assumed that the same situation applies for chemisorption on cobalt. The results presented in the next section on temperature effects also provide evidence that the assumption is valid in the temperature range —34 to 75°C.

Temperature Effects

A numerical requirement of the chromatographic method is that the moments be large enough for accurate measurement and yet not show excessive tailing, which would introduce large uncertainties in the second moment. Preliminary measurements were made from —34 to 300°C to study the nature of the chromatographs. From the first moment, K_a can be calculated [by Eq. (11)]. Then n_a is obtained by multiplying by C. If the chromatographic runs are at equilibrium conditions, this value of n_a will be the equilibrium adsorption. Figure 4 shows n_a values so calculated from first moments. In the temperature range —34 to 75°C, the results are as expected according to Fig. 1; K_a and n_a change but slowly with temperature. However at temperatures above 75°C there is a dramatic increase in n_a. This increase is the opposite of that expected if equilibrium existed at the chromatographic peak. Experimentally, extensive tailing was observed at these temperatures. Similar behavior has been noted for nickel by Ozaki *et al.* (*4, 5*). It is believed due to the availability of tightly-bound hydrogen, which does not participiate in the exchange reaction at lower temperatures. Possibly this could involve hydrogen bound to the catalyst support (*1*). In any event the required linear relation between C and n_a is not satisfied at temperatures above about

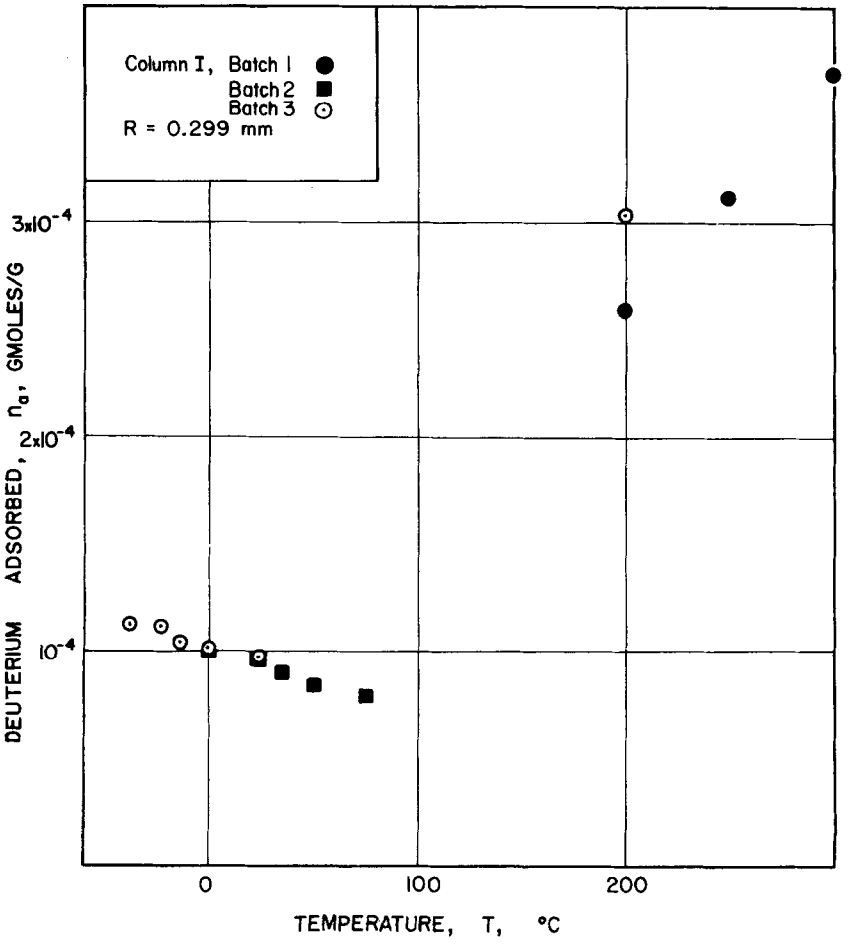

FIG. 4. Dynamic uptake of hydrogen vs. temperature.

75°C. Hence, the final data were taken at temperatures between —34 and 23.5°C. It may be noted that Ozaki found good agreement between n_a values for nickel obtained by static equilibrium measurements and obtained chromatographically. The agreement at high temperatures was poor.

FIRST-MOMENT ANALYSIS

Equation (3) is the first absolute moment of deuterium for the column. In contrast, μ_1' determined from the chromatographic peak and Eq. (7) includes the retention time in the dead space between detector and column, and between pulse injection and column. If this dead volume is V_d and the volumetric flow rate is F, Eq. (3), combined with Eq. (5), gives for μ_1'

$$\mu'_1 = \frac{z}{v}\left(\frac{1-\alpha}{\alpha}\beta\right)\frac{\rho_p}{\beta}K_a + \frac{z}{v}\left(1+\frac{1-\alpha}{\alpha}\beta\right)+\frac{t_0}{2}+\frac{V_d}{F}. \quad (9)$$

Since $K_a = 0$ for a nonadsorbable gas, the measured first absolute moment for helium is equal to

$$(\mu')_{He} = \frac{z}{v}\left(1+\frac{1-\alpha}{\alpha}\beta\right)+\frac{t_0}{2}+\frac{V_d}{F}. \quad (10)$$

Subtracting the deuterium and helium moments gives

$$\frac{\Delta\mu'_1}{\beta(1-\alpha)\alpha} = \frac{\mu'_1-(\mu'_1)_{He}}{\beta(1-\alpha)\alpha} = \left(\frac{\rho_p}{\beta}K_a\right)\frac{z}{v} \quad (11)$$

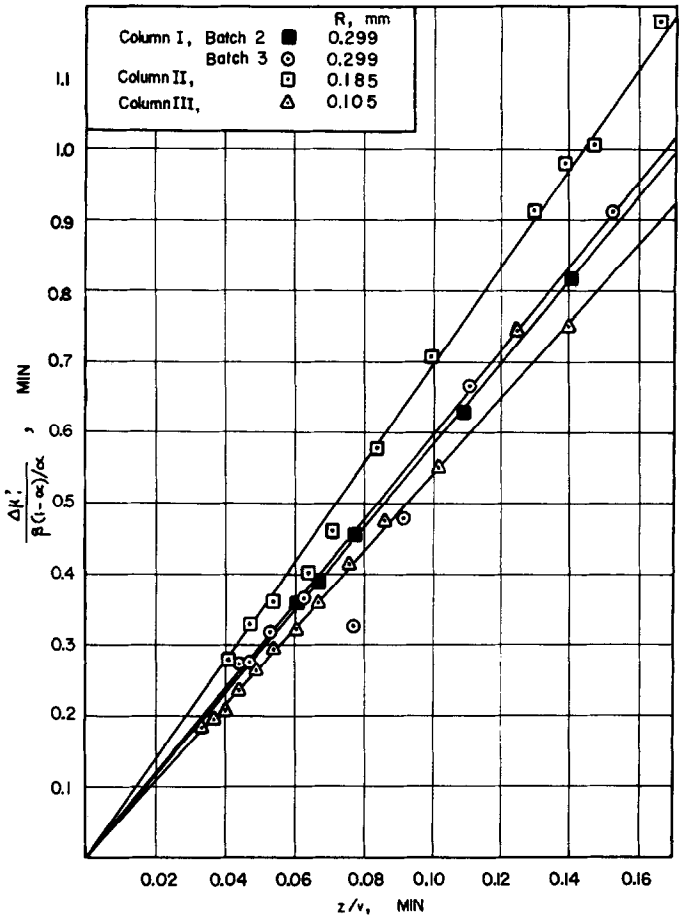

FIG. 5. First moment lines for different particle sizes at 0°C.

From the chromatographs a value of the left side of Eq. (11) is known for each z/v. The results, illustrated in Fig. 5 for 0°C, show the required linear relationship although there is some unexpected variation in slope with particle size. These variations may arise from errors in porosity measurements and slight differences in catalyst capacity, due to differences in extent of reduction. The data in Fig. 5, which are typical of that for other temperatures, give slopes of 5.5, 7.0, and 5.9 for $R = 0.105$, 0.185, and 0.299 mm, respectively.

For each temperature the average slope, equal to $(\rho_p/\beta)\ K_a$, was obtained for the three particle sizes and a corresponding value of K_a was evaluated. The equilibrium adsorption of hydrogen, n_t, is obtained by multiplying K_a by the gas concentration C_t. The latter is evaluated at column pressure (779 mm) and temperature. These results are shown in Table 3. In the last column K_a for hydrogen on the nickel–kieselguhr catalyst (*6*) is given. It is 4–5 times as large as K_a for the cobalt catalyst. Little information is available on the rela-

TABLE 3
PSEUDO-EQUILIBRIUM CONSTANTS AND ADSORPTION CAPACITY

	Cobalt catalyst		Nickel catalyst (*6*)
Temp (°K)	K_a (cm³/g)	n_t (10^{-4} g mole/g)	K_a (cm³/g)
296.5	2.29	0.941	11.1
273	2.21	0.987	10.9
259	2.18	1.026	
250	2.22	1.082	10.8
239	2.15	1.096	

tive adsorption capacities of nickel and cobalt. Ozaki *et al.* (*6*) have measured (by chromatography) the equilibrium adsorption of hydrogen over a wide temperature range for cobalt-on-kieselguhr and for Raney nickel. Schuit and Van Reijen (*10*) give the ratios of hydrogen uptake per metal atom of different catalysts. On a basis of unity for cobalt, their result for nickel is 2.3. If this ratio is arbitrarily corrected in a linear way for differences in metal content (50 vs. 74 wt %) and surface area (205 vs. 77 m^2/g) of the two catalysts, it becomes 4.1. This agrees roughly with the ratios of the K_a values given in Table 3.

The nearly constant K_a over the range —34 to 23.5°C indicates that the cobalt surface is essentially saturated with hydrogen, as suggested by Fig. 1.

Second-Moment Analysis

In principle, an additional term should be added to Eq. (4) to account for the dispersion in the dead volume. However, experiments with deuterium pulses when the column was bypassed indicated that dispersion in the dead volume was always less than 3% of the total second moment. Hence, Eq. (4) was used as given. Rearrangement gives

$$\frac{\mu_0 - t_0^2/12}{2z/v} = \delta_1 + E_A \frac{(1+\delta_0)^2}{\alpha} \frac{1}{v^2} \qquad (12)$$

The second-moment data for the three particle sizes are plotted versus $(1/v)^2$ in Figs. 6–8, and straight lines are obtained. Equation (6) shows that δ_1 is a function of k_f, and this is, in general, a function of velocity. However, the contribution of the term $5/k_fR$ in Eq. (6) is much less than that of $1/D_i$ at the conditions of these experiments. Hence, δ_1 is essentially independent of velocity so that the straight lines in Figs. 7–9 are expected from Eq. (12). The second term of this equation represents the dispersion of deuterium in the gas phase of the column. From the slopes of the lines in Figs. 7–9, the axial diffusivity E_A can be evaluated, using for δ_0 the values

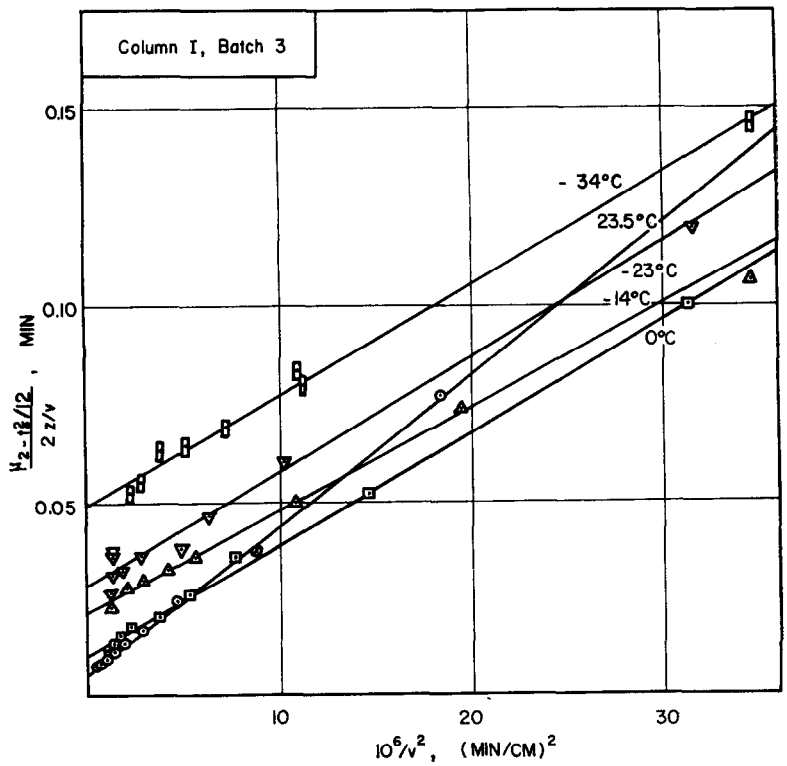

FIG. 6. Second-moment lines for different temperatures (R = 0.299 mm).

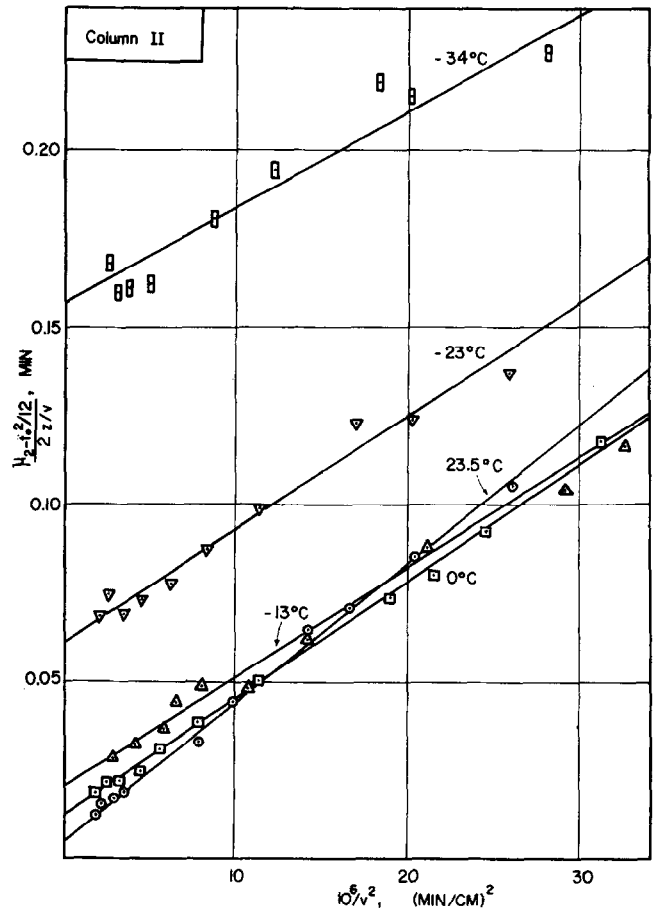

FIG. 7. Second-moment lines for different temperatures (R = 0.185 mm).

calculated from Eq. (5) with K_a taken from Table 3. The resultant E_A varied from 0.46–0.71 cm²/sec over the temperature range. Using estimated molecular diffusivities for hydrogen, from the Chapman-Enskog Eq. (2), and calculating tortuosity

$$E_A = \frac{\alpha D_{H_2}}{q_{ext}}, \qquad (13)$$

factors from the expression, showed q_{ext} to vary from 0.8 to 0.94. These relatively low values suggest that there was some dispersion due to turbulence in the bed. The particle Reynolds numbers in the column ranged from 0.04 to 1.9.

Our main interest is in the intercepts of Figs. 7–9 for they give δ_1 which includes the desired adsorption rate constant k_a. The accuracy with which k_a can be evaluated depends upon the magnitude of the intercept, and how precisely it is established. The figures indicate that, except at the highest temperature, the intercepts are relatively large so that reasonably accurate values of k_a are possible.

According to Eq. (6) graph of $\{\delta_1/[(1-\alpha)\beta/\alpha]\}$ vs. R^2 at a constant temperature should be linear and with intercepts equal to $(\rho_p/\beta)K_a^2/k_a$. The data are so plotted in Fig. 9. While the points scatter, particularly at the lower temperatures, relatively flat lines are obtained so that the intercepts are well established. Table 4 gives k_a determined from these intercepts. The rates of adsorption, or desorption, of hydrogen are equal to k_a multiplied by the concentration C_t, and these

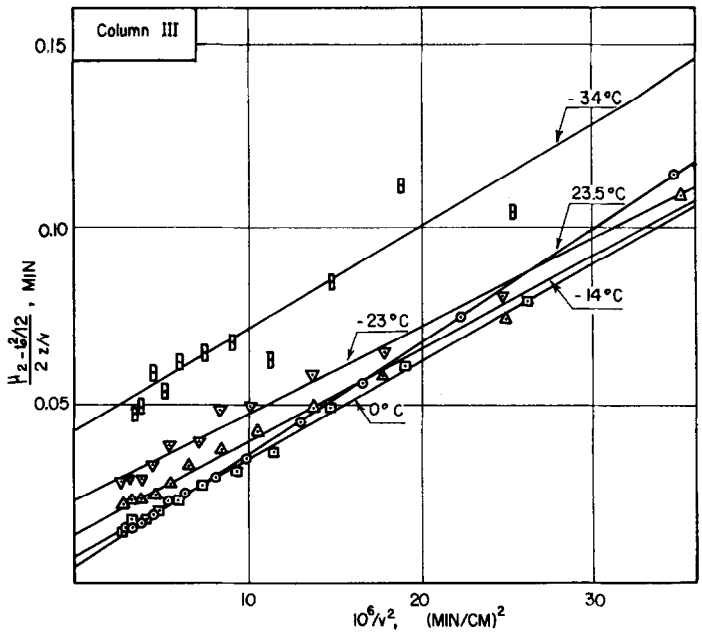

FIG. 8. Second-moment lines for different temperatures (R = 0.105 mm).

rates are also shown in Table 4. Table 4 provides the major results of this study.

Equation (6) shows also that the slope of the lines in Fig. 9 is a measure of $(1/D_i + 5/k_f R)$. Since the contribution of external diffusion is a small part (10–15%) of the intraparticle diffusion resistance, and since the Reynolds number is low, $5/k_f R$ may be adequately approximated by taking $k_f = D_{H_2}/R$. This corresponds to external mass transfer being entirely by molecular diffusion; i.e., $k_f(2R)/D_{H_2} = 2$. Then, from the slope of the lines, D_i is about 3×10^{-2} cm^2/sec. The scatter of the data points in Fig. 9 prevents establishing separate slopes for each temperature. Hence, this diffusivity

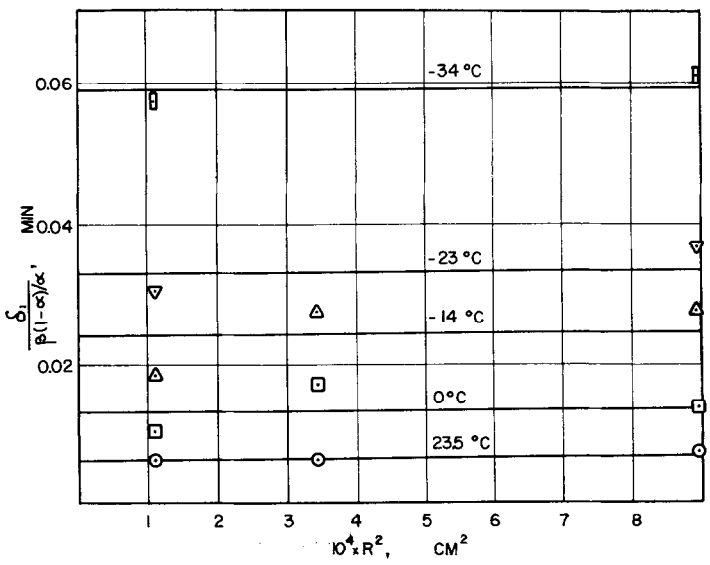

FIG. 9. Effect of particle size on second-moment function.

TABLE 4
ADSORPTION RATE CONSTANTS

Temp (°K)	k_a (cm³/g mole)	Rates of adsorption (or desorption) of hydrogen [g moles/(g)(sec)]	
		Cobalt (this work)	Nickel (6)
296.5	37.6	1.6×10^{-3}	1.0×10^{-2}
273	16.7	7.6×10^{-4}	2.9×10^{-3}
259	8.99	4.3×10^{-4}	
250	6.82	3.4×10^{-4}	3.0×10^{-4}
239	3.59	1.9×10^{-4}	

is an average and approximate result over the range —34 to 23.5°C. The predicted intraparticle diffusivities from the random pore model (7), using the porosity and pore radii given in Table 1, range from 3.3×10^{-2} at 23.5°C to 2.9×10^{-2} cm²/sec at —34°C. The agreement is better than expected. It should be emphasized that the conditions of the experimental work were not chosen so as to evaluate accurate diffusivities, but to obtain adsorption rate constants. To determine D_i with confidence, the slope or abscissa range of Fig. 9 should be larger with respect to the intercept. This could be achieved by experiments at higher temperatures with larger particles as illustrated by Schneider and Smith (8).

DISCUSSION

Figure 10 is an Arrhenius plot of the rate data (Table 4) according to the equation

$$r_a = r_d = A \exp\left(-\frac{E}{R_g T}\right). \qquad (13)$$

A least-mean-square fit of the points gives an activation energy of 5.2 kcal/g mole. This value represents the combined temperature dependency of the separate factors

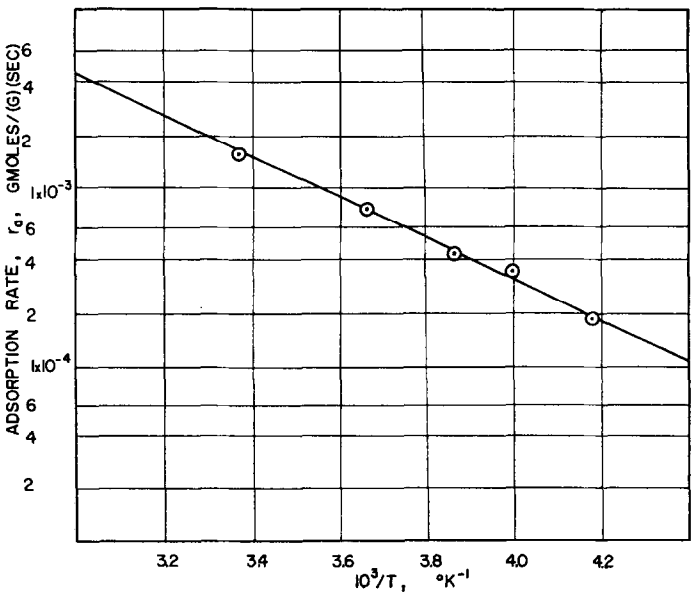

FIG. 10. Arrhenius plot of adsorption rates.

in a theoretical rate equation of the transition-state type. For desorption such a theoretical relation would be written as

$$r_d = \frac{n_s \varphi(\theta)}{2} \left(\frac{k_B T}{h}\right) \Phi(f) \left(\exp - \frac{E_d}{R_g T}\right), \tag{14}$$

where n_s is the total available sites per gram of catalyst, $\Phi(f)$ is a function of the partition function of the activated complex and that of a pair of adsorbed hydrogen atoms, and $\varphi(\theta)$ is the probability that pairs of atoms are adsorbed on adjacent sites. Under the experimental conditions of this work, the surface is nearly fully covered. Hence θ is about independent of temperature. Further the small effect of temperature on $\varphi(\theta)$ tends to be balanced by $k_B T/h$. Also the adsorbed atoms and the activated complex are likely to be immobile (*9*). Hence, the partition functions are due only to vibrations so that $f \approx 1$ and $\Phi(f) \approx 1$. Thus, the only factor in Eq. (14) which is strongly temperature dependent is the exponential one. Comparison of Eqs. (13) and (14) indicates that the observed E must correspond closely to the activation energy for desorption.

By similar reasoning Padberg and Smith (*7*) obtained an activation energy for desorption for nickel-on-kieselguhr of 13.8 kcal/g mole. The heat of adsorption for hydrogen on Ni/kieselguhr catalyst was available and equal to 13.5 kcal/g mole. Hence, it was concluded that the chemisorption of hydrogen on nickel was essentially nonactivated ($E_a \approx 0$), since

$$E_a = E_d + \Delta H_a. \tag{15}$$

Unfortunately, ΔH_a for a cobalt/kieselguhr catalyst was not available in the literature so a similar statement cannot be made. It is clear from a comparison with Padberg's results that the two rates of adsorption are about the same at low temperatures (~—30°C) but that the adsorption on cobalt is an order of magnitude slower at room temperature. The variation in surface areas between the catalysts is too small to explain this difference.

Finally, the possibility of an isotope effect on the rate should not be ignored. If such an effect is significant (ratios of hydrogen to deuterium rates of 1.3–2.5 have been reported (*11*) for gaseous reactions of the two molecules) the data presented here refer to deuterium rather than hydrogen.

Acknowledgments

The financial assistance of the National Science Foundation, Grant GK-2243, is gratefully acknowledged.

References

1. Eischens, R. P., and Pliskin, W. A., *Advan. Catal. Relat. Subj.* **10**, 32 (1958).
2. Hirshfelder, J. O., Curtis, C. F., and Bird, R. B., "The Molecular Theory of Gases and Liquids." Wiley, New York, 1954.
3. Kubin, M., *Collect. Czech. Chem. Commun.* **30**, 1104, 2900 (1965).
4. Ozaki, A., Nozaki, F., Maruya, K., and Ogasawara, S., *J. Catal.* **8**, 234 (1967).
5. Ozaki, A., Shigehara, Y., and Ogasawara, S., *J. Catal.* **8**, 22 (1967).
6. Ozaki, A., and Shigehara, Y., *J. Chem. Soc. Jap.* **88**, 844 (1967).
7. Padberg, G., and Smith, J. M., *J. Catal.* **12**, 172 (1968).
8. Rao, M. R., and Smith, J. M., *AIChE J.* **9**, 485 (1963).
9. Schneider, P., and J. M. Smith, *AIChE J.* **14**, 762 (1968).
10. Schuit, G. C. A., and Van Reijen, L. L., *Advan. Catal. Relat. Subj.* **10**, 242 (1958).
11. Wiberg, F., *Chem. Rev.* **55**, 736 (1955).